Environ Geochem Health (2023) 45:7131–7144
https://doi.org/10.1007/s10653-023-01655-z

ORIGINAL PAPER

Removal of cobalt and strontium by adsorption using Brewer's spent grain formed by pyrolysis

Hyung Wook Lee · Han Gyeol Jeon · Kyoung-Woong Kim

Received: 27 February 2023 / Accepted: 7 June 2023 / Published online: 17 June 2023

Abstract One byproduct of brewing beer is Brewer's spent grain (BSG), which is reused in animal feed. However, BSG has valuable potential for other products such as biochar because of its high protein and fiber content. Radioactive waste is one of the biggest concerns in Korea because of the permanent shutdown of the Gori nuclear power plant. In this study, we aimed to use BSG-850, a biochar originating from BSG after pyrolysis at 850 °C, for the adsorption of cobalt (Co) and strontium (Sr), which are two radionuclides that contribute to radioactive waste. The adsorption capacity of Co and Sr was reinforced with increased temperature which are 3.304, 4.659, 5.516 mg/g (Co) and 1.462, 2.54, 3.036 mg/g (Sr) at 298, 308, and 318 K, respectively. The reusability of BSG-850 capacity was 75.3, 47.8, 43.6, 36.2% and 93.6, 84.2, 57.2, and 32.7% after 1, 2, 3, and 4 cycles, for Co and Sr, respectively. In the presence of other competitive ions, the adsorption capacity decreased. The adsorption capacity and properties of BSG-origin biochar for Co and Sr were confirmed and BSG can be a desirable option for solving radioactive waste issue.

H. Lee · H. Jeon · K.-W. Kim (✉)
School of Earth Sciences and Environmental Engineering, Gwangju Institute of Science and Technology (GIST), Gwangju 61005, Republic of Korea
e-mail: kwkim@gist.ac.kr

Keywords BSG · Biochar · Co · Sr · Radioactive waste · Radionuclide · Adsorption · Pyrolysis · Aqueous solution

Introduction

Beer is one of the most popular drink worldwide and it is easy to make with low cost than other liquors. Beer is made from several ingredients such as grains, yeast, hops, water, and other additives. The first step of brewing beer is malting; during this process, amylase in barley converts starch to sugar to create maltose. The next step is mashing, where the malt is boiled with water to extract the sugar from the malt. After mashing, the sugar-containing water, called wort, eventually becomes beer, and the used barley becomes a byproduct called Brewer's spent grain (BSG). According to Musatto et al. (2006), the mashing step produces the most BSG, and BSG corresponds to 85% of the total generated byproducts.

The simplest and easiest way to reuse BSG is through animal feed. Even though sugar is extracted during the mashing process to brew the beer, BSG has a high protein and amino acid content. Also, BSG is cheap and easy to obtain due to the popularity of beer. In addition to animal feed, BSG can also be used as an additive in bakery and paper production (Bachmann et al., 2022). This study focuses on using BSG as an adsorbent to be used in the removal of cobalt

(Co) and strontium (Sr) in aqueous solution to resolve environmental and radiation problems.

Currently, the world faces a serious environmental crisis due to global warming and climate change. Most governments in developed countries and environmental organizations such as the Intergovernmental Panel on Climate Change (IPCC) claim that CO_2 production in human society at present is dangerous and CO_2 production must be reduced as soon as possible. Moreover, the IPCC recommends that the temperature rise must be below 1.5 °C compared to the pre-industrialization era (1850–1900) at their report (Masson-Delmotte et al., 2018). However, the Earth's temperature has already increased by 1 °C, and the Earth's temperature will increase by 1.5 °C in 2030–2052 if this trend continues. To meet the IPCC recommendation, CO_2 production in the world must be reduced 45% by 2030, compared to 2010 levels according to their report.

To help resolve the CO_2 production problem, pyrolysis can be utilized as an effective method for disposing waste. Pyrolysis is a combustion process that occurs under non-oxygen or low-oxygen conditions. Through pyrolysis, it is possible to reduce the amount of the final waste product, reduce the amount of toxic chemicals such as dioxin, and diminish the size of the required waste disposal facilities. Compared with the general incineration process, the generation of biochar using pyrolysis can reduce CO_2 production. Biochar is a compound word (biomass + charcoal) produced by pyrolysis using biomass such as food, agriculture, and forestry waste. This BSG is similar to agricultural waste because it mainly consists of cellulose, protein, and lignin like other grains. Therefore, the production of BSG-origin biochar by pyrolysis is significantly valuable not only as a method for reusing BSG effectively, but also for solving the global environmental crisis.

Another environmental issue in Korea is the radiation related to Japan. In 2011, due to an earthquake and tsunami, 4 nuclear reactors were destroyed at the Fukushima nuclear power plant (NPP), resulting in the release of radioactivity into the adjacent air and water. The Japanese government and International Atomic Energy and Agency (IAEA) estimated the Fukushima NPP accident to be grade 7. On July 22 in 2022, the Japan Nuclear Regulation Authority (NRA) approved the disposal of contaminated water produced during the treatment of the Fukushima NPP to the ocean. However, the Japanese government and NRA did not disclose the concentration of radioactive compounds in the water to the public. The Fukushima NPP accident and the disposal of contaminated water remind us of the importance of regulating and treating radioactive waste.

The liquid-state radioactive waste was treated via concentration and evaporation. The concentrated liquid waste was placed into a safe storage container after the solidification process and dumped underground with other solid radioactive waste. After treatment, the concentration of radioactive compounds in water must be measured and disposed of in the ocean under safe conditions. Radiation from radioactive elements or contaminated waste is extremely dangerous. It is impossible to observe radiation with the naked eye or determine whether our body is exposed to radiation. Moreover, damage from radiation is expressed after a long period of time and can affect the future generations. Therefore, all countries that operate NPPs, including Korea, need to strictly regulate the radiation and disposal of radioactive waste.

According to previous research, BSG has an adsorption capacity for heavy metals, such as lead (Kwak et al., 2019), chromium (Vanderheyden et al., 2018), manganese, zinc, nickel, cadmium, and copper (Wierzba & Kłos, 2019). However, research on the adsorption capacity of both cobalt (Co) and strontium (Sr) using the same type of BSG is rare and the contaminated water produced from NPPs contains several elements. Thus, the adsorption capacity of BSG with other competitive elements should be studied for application in the field to determine the potential of BSG-origin biochar for treating contaminated water in NPPs.

Materials and methods

Preparation of samples

The BSG was purchased from a commercial company named Han-Joon SS, which brought BSG from the OB Beer Company, Korea, to the online market. The BSG was dried in an oven at 70 °C for 3 days to remove moisture and prevent decay by microorganisms. Dried BSG was crushed to a powder form using a ball mill machine (Pulverisette 5, Fritsch). The crushed BSG was separated by a 200 μm sieve,

and only BSG below 200 μm in size was used for the experiment. Raw BSG (BSG-R) represents BSG before the pyrolysis process.

To reduce the release of toxic materials and the volume of the product, BSG was converted to biochar by pyrolysis under anaerobic conditions. To ensure anaerobic conditions, all gases in the furnace were vented first. N_2 gas was then injected into the vacuum state of the furnace until the N_2 pressure reached 1 bar. After N_2 gas injection, the pyrolysis process was initiated. The activation temperatures of the pyrolysis process were 450, 650, and 850 ℃; 450 °C was chosen because the minimum temperature of pyrolysis is approximately 450–500 ℃, and the other temperatures were chosen to assess the effect of different activation temperatures on the biochar products. The temperature was increased at a rate of 5 °C/min and maintained for 1 h when the activation temperature was reached. After the furnace and sample were cooled to room temperature, the sample was removed and separated by a 200 μm sieve. After pyrolysis, BSG was named according to the activation temperature as BSG-450, BSG-650, or BSG-850, and all types of BSG, including BSG-R, were stored in a desiccator to maintain a consistent humidity.

Chemicals

Cobalt nitrate heptahydrate ($Co(NO_3)_2$-$7H_2O$, Sigma Aldrich) and strontium nitrate ($Sr(NO_3)_2$, Sigma-Aldrich) were used to prepare stock solutions for each element in all adsorption experiments. Manganese nitrate tetrahydrate ($Mn(NO_3)_2$-$4H_2O$, Sigma-Aldrich), cadmium nitrate tetrahydrate ($Cd(NO_3)_2$-$4H_2O$, Sigma-Aldrich), nickel nitrate hexahydrate ($Ni(NO_3)_2$-$6H_2O$, Sigma Aldrich), and sodium chloride (NaCl, Merck) were used to prepare stock solutions for each element in the competitive adsorption experiment. To adjust the pH, sodium hydroxide (NaOH, Sigma Aldrich) and 70% nitric acid (HNO_3, Daejung) were used. ICP multi-element standard solution IV (1.11355.0100, Merck) was used to measure the Co and Sr concentrations of the samples.

Characteristics of BSG

In order to determine sample characteristics, 2 g of a BSG sample was added to 10 mL of distilled water (1:5 g/mL) and mixed at 150 rpm for 15 min. After mixing, the sample was centrifuged at 3000 rpm for 5 min, and the pH of the supernatant was measured using a pH meter (Thermo Orion 720 A + , USA).

For cation exchange capacity (CEC) analysis, 1 M of NH_4OAC (pH 7.0) was passed through the soil to concentrate the cation exchange charges to NH_4^+ and washed with 95% ethanol solution. Then, MgO was added to the NH_4^+-concentrated soil, distilled, and collected by NH_3 gas using a Kjeldahl distiller. Finally, CEC was measured by titration using an acid solution. CEC analysis was performed by the Seoul Green Bio Research Facility Center (GBRFC).

Determination of the existence and distribution of the surface functional groups in BSG, Fourier-transform infrared spectroscopy (FT-IR) analysis was performed using a spectrophotometer (Bruker Vertex 70v, USA) using the attenuated total reflection (ATR) method (crystal: Ge, refractive index = 4.0). Brunauer–Emmett–Teller (BET) analysis was conducted on the four types of BSG to assess the difference in surface structure and pore size using Micromeritics Tristar II 3020 (USA). Before analysis, all samples were dried under a vacuum at 70 °C for 24 h to remove moisture. After pretreatment, N_2 gas was used as the adsorption gas. BET analysis was performed by the Korea Polymer Testing and Research Institute (KOPTRI). Scanning electron microscope (SEM) analysis was conducted to confirm whether each type of BSG had a different surface structure (HITACHI High Tech Co.. S-4800 cold type, Japan), and the elemental composition was determined using an elemental analyzer (Elementar UNICUBE, USA).

Effect of pH

To avoid the removal of Co and Sr by precipitation rather than adsorption, all experiments were conducted at pH < 8. The pH of the Co and Sr stock solutions (initial concentration:10 ppm) was adjusted to a pH of 2, 3, 4, 5, 6, and 7 using 0.1 M NaOH or 0.1 M HNO_3. Four types of BSG (0.05 g) were added to 40 mL of stock solutions of different pH levels (1.25 g/L ratio) and shaken at 200 rpm for 24 h at 298 K. After shaking, the BSG-containing liquid was filtered through a 40 μm PTFE syringe filter to prevent additional adsorption. The filtered liquid was stored at room temperature and the concentrations of Co and Sr in the aqueous solution were measured. All the processes for the pH experiment were duplicated.

Adsorption experiment

For the adsorption kinetic experiments, 2 L of Co and Sr stock solutions were prepared (initial concentration:10 ppm), the pH was adjusted to 7, and only BSG-850 was used. A 2.5 g BSG-850 sample was mixed with 2 L of Co and Sr stock solutions (1.25 g/L ratio). The mixtures were shaken at 400 rpm at room temperature for 48 h. During shaking, 5 mL of the sample was removed at specific times and filtered using a 40 µm PTFE syringe filter to prevent additional adsorption. The filtered liquid was stored at room temperature and the concentrations of Co and Sr in the aqueous solution were measured. All the processes for the adsorption kinetic experiments were duplicated, and the concentration change of Co and Sr was applied to the pseudo-first model (PFO) and the pseudo-second model (PSO) to determine which model was appropriate for Co and Sr adsorption. The specific equations for the PFO and PSO models and the calculation of the adsorption capacity are:

$$\text{PFO model}: \ Q_t = Q_e\left(1 - \exp^{-Kt}\right) \tag{1}$$

$$\text{PSO model}: \ Q_t = Q_e^2 Kt \,/\left(1 + Q_e Kt\right) \tag{2}$$

$$Q_e = \left(C_0 - C_t\right) \text{V/m} \tag{3}$$

where Qe is the adsorption capacity at equilibrium, Qt is the adsorption capacity at time t, and K is the kinetic constant. The adsorption capacity was calculated by multiplying the volume of the stock solution (V) by the change in concentration ($C_0 - C_t$) and dividing by the weight of the used BSG (m).

For the adsorption isotherm experiments, the pH of the Co and Sr stock solutions was adjusted to 7, and only BSG-850 was mixed with the stock solutions. A 50 mg BSG-850 sample was mixed with 40 mL of Co and Sr stock solutions. The initial concentrations of the Co and Sr stock solutions were 1, 2.5, 5, 10, 25, 50, and 100 ppm. The mixtures were shaken at 200 rpm at 298 K for 24 h. After mixing, the change in concentration was measured, and the data were applied to the Langmuir and Freundlich models to determine the maximum adsorption capacity (Qe) and properties of adsorption with BSG. All other experimental procedures were the same and duplicated.

Effect of temperature, competitive ions and bio-regeneration

The experimental design conditions for the effect of temperature experiments were the same as the adsorption isotherm experiments with the exception of the temperature conditions. The adsorption temperatures were 298, 308, and 318 K, respectively and all experiments are duplicated.

For the competitive ion experiments, nickel (Ni), manganese (Mn), cadmium (Cd), and sodium (Na) were selected because of their relatively short half-lives compared to that of other radionuclides. Each element was added to the Co and Sr stock solutions, and the change in concentration after the adsorption process was measured by comparison with adsorption isotherm data. All the processes for the competitive ion experiments were duplicated.

After one adsorption process, the BSG was desorbed using 0.01 M HNO_3 under the same experimental conditions, such as pH, adsorption time, or temperature. The 2nd adsorption process followed the 1st desorption. In total, five adsorption processes were conducted, and the maximum adsorption capacities at each step were compared. All the processes for the bio-regeneration experiments were duplicated.

Results and discussion

Properties of BSG

After the pyrolysis process, all BSG types (BSG-450, BSG-650, and BSG-850) had a black color, whereas the original state of BSG and BSG-R had a yellow–brown color (Fig. 1). The pH and CEC were measured as the fundamental chemical properties of all BSG types and are described in Table 1. As the pyrolysis temperature increased, both the pH and CEC decreased. This is because the surface functional group, the most important parameter in determining pH and CEC, disappeared with a high level of pyrolysis in BSG-650 and BSG-850 (Tomczyk et al., 2020).

FT-IR spectroscopy was used to confirm the surface functional groups of BSG, and the results are shown in Fig. 2. BSG-R has several peaks such as the O–H bond (3300 cm^{-1}), C=O bond (2920, 2360, and 1740 cm^{-1}), C-H bond (2850 cm^{-1}), and C-O

Fig. 1 Images of BSG: original state, BSG-R, BSG-450, BSG-650, BSG-850 (from the left)

Table 1 Physicochemical characterizations of all BSGs: pH, CEC, surface area and pore volume

BSG type	pH	CEC (meq/100 g)	Surface area (m^2/g)	Pore volume (cm^3/g)
BSG-R	5.26	42.5	1.13	0.003
BSG-450	6.74	33.7	2.33	0.0059
BSG-650	7.93	19.9	248	0.13
BSG-850	8.58	14.5	394	0.21

bond (1240 and 1030 cm^{-1}). Among them, the O–H bond at 3300 cm^{-1}, and the C-O bonds at 1240 and 1030 cm^{-1} are common peaks on biomass material, which indicate the vibration of the OH group of cellulose, the C-O stretching of lignin, and the C-O stretching of hemicellulose, respectively (Balogun et al., 2017; Hassan et al., 2020). Thus, the main components of BSG were cellulose, hemicellulose, and lignin, as confirmed by the literature review and the results of the FT-IR analysis of BSG-R.

The decrease in surface functional groups was also confirmed by FT-IR analysis. When the pyrolysis was performed at 450 °C, the surface functional group decreased compared to the raw state. In the graph (Fig. 2), BSG-450 has similar peaks to BSG-R, but has a lower absorbance value, which indicates a decrease. Previous research has explained that this result is due to the breakage of functional groups during the pyrolysis process (Balogun et al., 2017; Tomczyk et al., 2020).

However, after pyrolysis at 650 and 850 °C, most of the peaks disappeared but had a higher absorbance compared to that of BSG-R and BSG-450. In addition, BSG 850 had a similar pattern and higher absorbance than BSG-650. This was due to the high

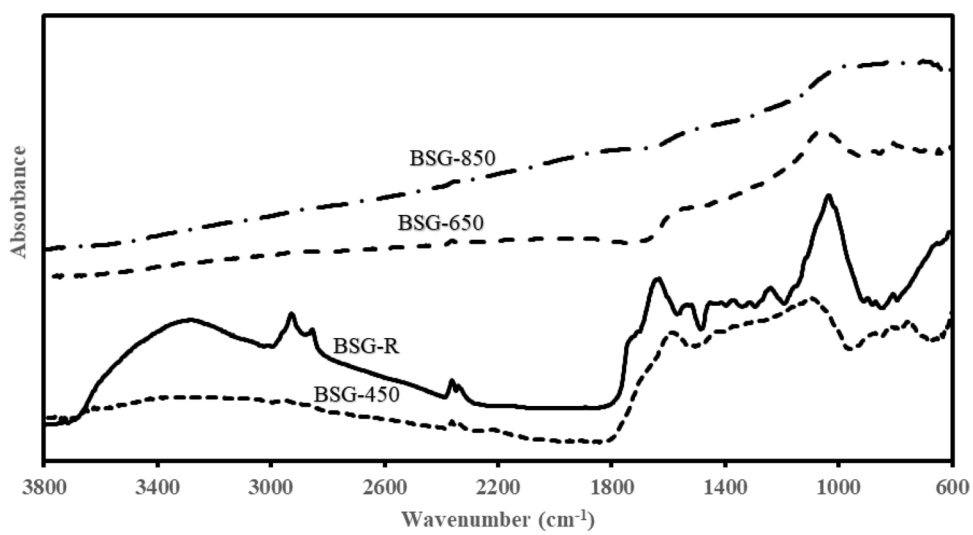

Fig. 2 FTIR spectra of four BSG types: BSG-R, 450, 650, and 850

pyrolysis temperature. When the pyrolysis temperature increases, the surface functional groups can disappear easily, and the biomass has well-organized carbon (C) layers, such as graphene and charcoal (Ahmad et al., 2014; Tomczyk et al., 2020). In addition, the increasing tendency of the absorbance baseline in BSG-650 and BSG-850 is significantly similar to that of natural graphite C (Liu et al., 2015). In conclusion, with both low- and high-temperature pyrolysis, the surface functional groups decreased, and BSG had well-organized C layers after high-temperature pyrolysis (650–850 ºC).

The surface areas and pore volumes of BSG-R, BSG-450, BSG-650, and BSG-850 were 1.13, 2.33, 248, 394 m^2/g and 0.003, 0.0059, 0.13, and 0.21 cm^3/g, respectively (Table 1). Both the surface area and pore volume increased with increasing pyrolysis temperature. This result is consistent with previous research on biochar, which explains that the results are due to the decomposition of organic matter and the production of micropores. In addition, several particles that block pores are thermally degraded, and the pores are exposed to an external surface during the pyrolysis process; volatile matter can be released, which can increase the pore volume and surface area (Kwak et al., 2019; Osman et al., 2019; Tomczyk et al., 2020).

In addition, BSG-650 and BSG-850 had a much larger surface area and pore volume than BSG-450, even though all three BSG types underwent pyrolysis. This suggests that BSG-650 and BSG-850 have graphite C properties, which were confirmed by the FT-IR analysis results above. A large surface area and pore volume are important for the adsorption capacity of BSG for metals.

Figure 3 shows SEM images of all BSG types at 5000 × magnification. BSG-R has a relatively smooth surface texture, while BSG-850 has the roughest texture visually. The SEM image at 15,000 × magnification is shown in Fig. 4, where different surface structures and pore distributions can be clearly observed. BSG-R has the lowest number of surface pores and BSG-850 has the highest number of the surface pores. These images are in good agreement with the BET analysis results in which BSG-R has the smallest surface area and pore volume (1.13 and 0.003 cm^3/g, respectively) and BSG-850 has the largest surface area and pore volume (394 m^2/g and 0.21 cm^3/g, respectively). These results are due to the degradation of pore-blocking materials and the removal of volatile matter, as explained above.

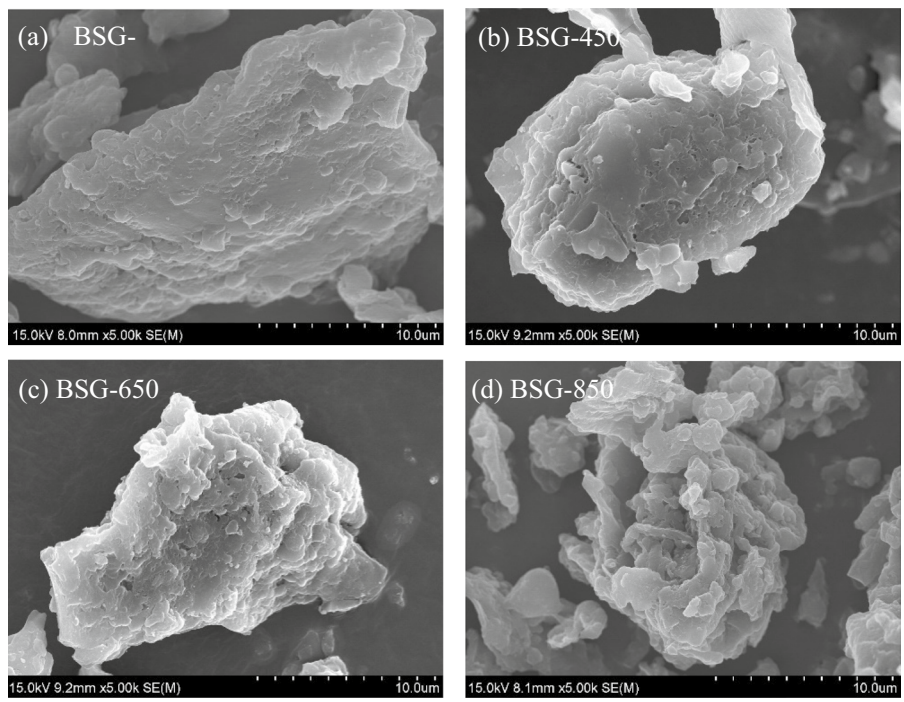

Fig. 3 SEM images of **a** BSG-R **b** BSG-450 **c** BSG-650 **d** BSG-850 (× 5,000)

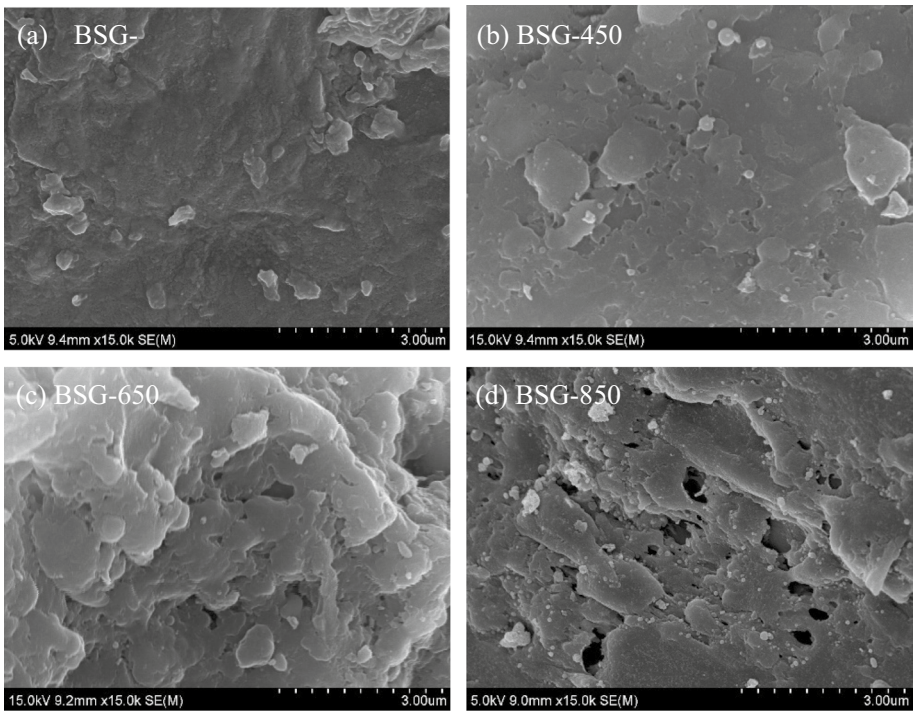

Fig. 4 SEM images of **a** BSG-R **b** BSG-450 **c** BSG-650 **d** BSG-850 (×15,000)

Figure 5 shows the SEM with energy dispersive X-ray analysis (SEM–EDX) images of BSG after the adsorption operation. In Fig. 5, Co was observed on the surface of BSG, indicating that the adsorption of Co by BSG was successful and Sr was also observed on the surface of BSG. SEM–EDX analysis confirmed that the removal of Co and Sr in the aqueous solution was due to adsorption by BSG.

When the pyrolysis temperature was increased, the composition of C increased significantly. The C composition was 45.88% in BSG-R but was 71.67% in BSG-850, and Table 2 shows the elemental compositions of the samples. Based on these results, a high pyrolysis temperature makes BSG similar to the graphite form of BSG, which is the same tendency discussed above.

The biochar yield was measured by comparing the weight of BSG before and after pyrolysis. BSG-450 had the highest yield at 54%, followed by BSG-650 at 27% and BSG-850 at 25%. The biochar yield decreased when the pyrolysis temperature increased, as shown in Table 2. This is because biochar has a more organized C layer under higher pyrolysis temperatures, which means it is more concentrated; this tendency was reported in a previous study, even though the degree of decrease varies (Li et al., 2019).

Effect of pH

Figure 6 shows the effect of pH on BSG-850. Among the four BSG types, only BSG-850 exhibited an adsorption capacity. This might be because the large surface area and pore volume play the most important roles in attaching metals to the BSG. BSG-850 did not have significant surface functional groups. In addition, in BSG-850, the adsorption capacity increased with increasing pH. This is due to the different concentrations of H + ions at different pH ranges. At low pH, the H^+ concentration is higher than that at higher pH, and H + disturbs the attachment of BSG between Co and Sr and cations such as H^+.

The maximum removal was observed at pH 7 using BSG-850 for both Co and Sr. The specific removal capacity was 3.17 mg/g of Co (40.4% removal efficiency) and 1.24 mg/g of Sr (15.5% removal efficiency) under the same experimental conditions (initial concentration: 10 ppm, mixing at 200 rpm, 298 K, BSG dosage: 1.25 g/L). In conclusion, only BSG-850

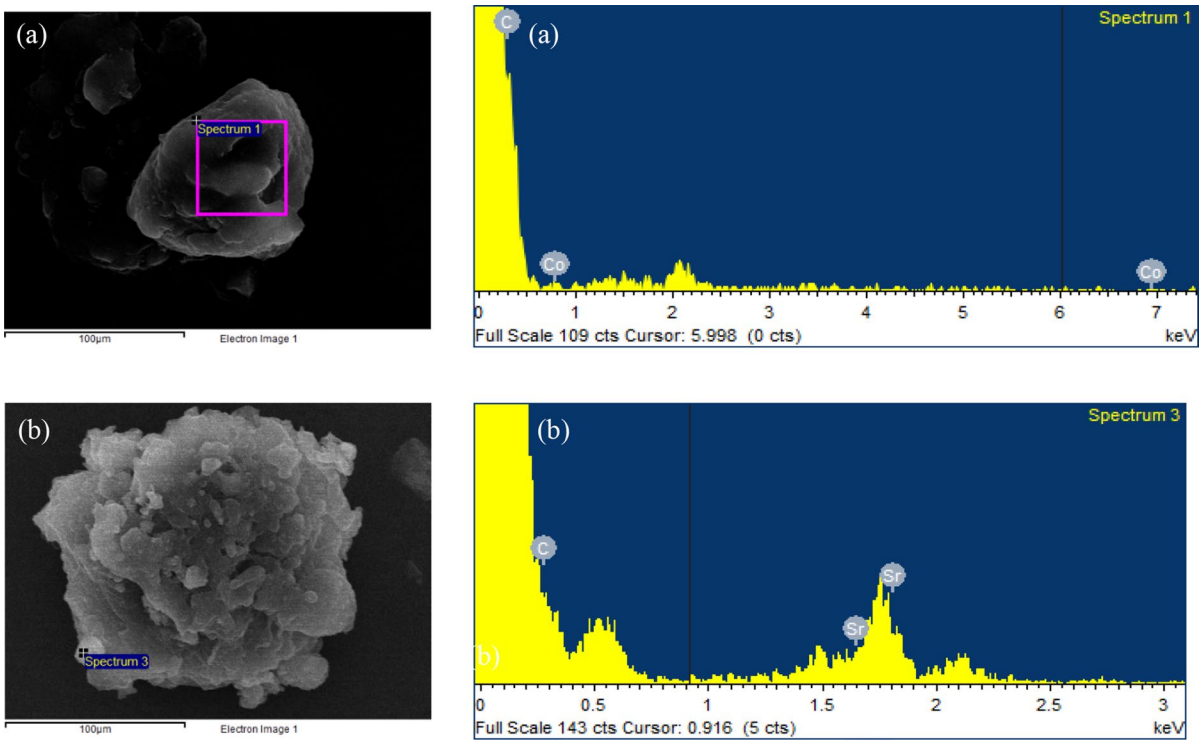

Fig. 5 SEM–EDX images of Co (**a**) and Sr (**b**) in BSG surface

Table 2 Elemental composition and biochar yield after pyrolysis

BSG type	Elemental composition (%)				Biochar yield (*w/w*, %)
	N	C	H	S	
BSG-R	3.43	45.88	6.62	0.43	–
BSG-450	4.43	67.22	3.22	0.17	54
BSG-650	2.59	69.34	1.8	0.1	27
BSG-850	2.03	71.67	1.26	0.08	25

had an adsorption effect, and the highest adsorption capacity was observed at pH 7 for both Co and Sr. Thus, the main adsorption experiment was performed at a pH of 7 to determine the maximum capacity.

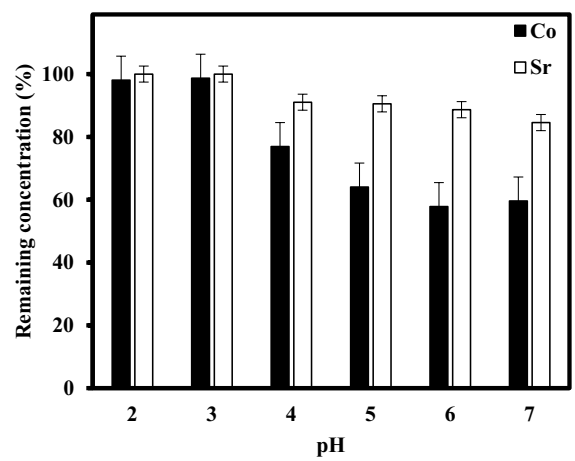

Fig. 6 The changes of the adsorption capacity of BSG-850 at various pH

Adsorption kinetics and isotherms

Among the PFO and PSO models, both Co and Sr kinetic data were well matched to the PSO model with R^2 values of 0.971 and 0.987, respectively, as described in Fig. 7. Table 3 shows several parameters for applying data to the PFO and PSO models. In addition, the adsorption equilibrium state was observed after 24 h of adsorption; therefore, the adsorption experiment was performed for 24 h.

The data from the adsorption isotherm experiments were fitted to Langmuir and Freundlich

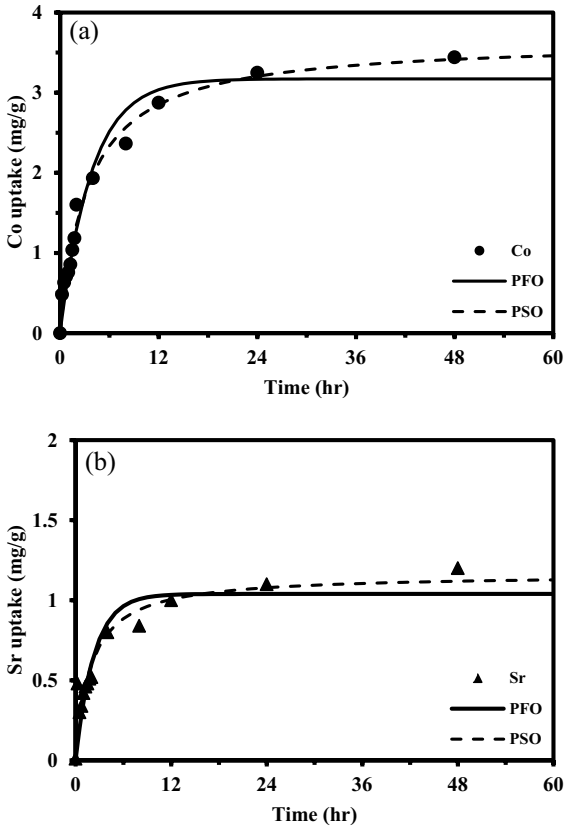

Fig. 7 Adsorption kinetic system: Co (**a**) and Sr (**b**)

Table 3 Summary of adsorption kinetics parameters

Models	Parameters	Adsorbates	
		Co	Sr
PFO model (pseudo-first order)	Q_e (mg/g)	3.172	1.391
	K_1 (L/min)	0.262	0.853
	R^2	0.971	0.886
PSO model (pseudo-second order)	Qe (mg/g)	3.304	1.462
	K_2 (L/min)	13.09	0.943
	R^2	0.987	0.948

models. According to the Freundlich model, the adsorption site of the adsorbent is heterogeneous, has multiple adsorption layers, and does not involve chemical forces. On the other hand, the Langmuir model has homogeneous adsorption sites, mono-adsorption layers, and chemical forces. The Freundlich model assumes an irreversible reaction, whereas the Langmuir model assumes a reversible reaction. The specific equations of the two models are described as:

$$\text{Freundlich model}: \ Q_e = K_F C_e^{1/n} \tag{4}$$

$$\text{Langmuir model}: \ Q_e = \left(Q_m K_L C_e\right)/\left(1 + K_L C_e\right) \tag{5}$$

where K_F and Q_m represent maximum adsorption capacities, $1/n$ is the adsorption strength, K_L represents the adsorption coefficient, and C_e and Q_e represent the mean concentration of adsorbates and adsorption capacity at a specific concentration, respectively (Langmuir, 1918; Qiu et al., 2013).

Figure 8 shows the results of the application of Co and Sr to both adsorption models. Among the two models, the Langmuir model was a better fit for both the Co and Sr results. The specific parameters of the adsorption model are described in Table 4. In conclusion, both Co and Sr follow the Langmuir model

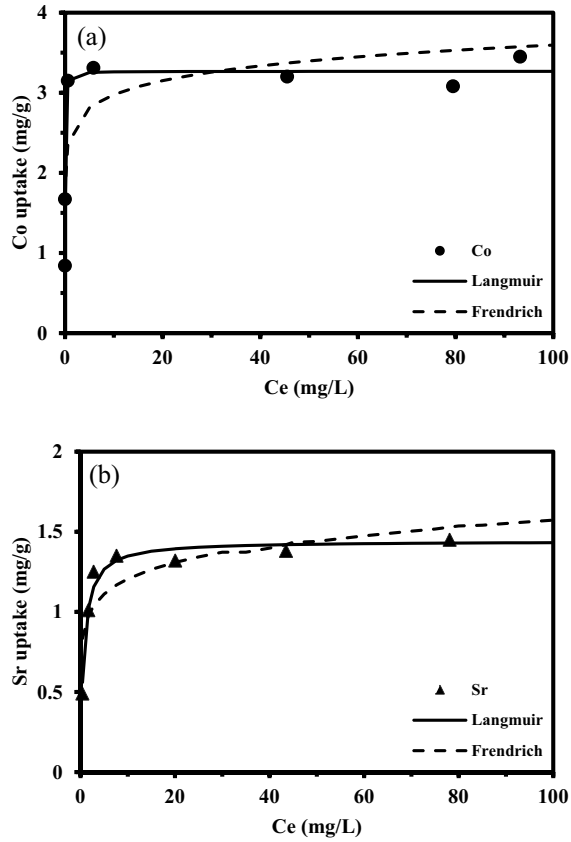

Fig. 8 Adsorption isotherm system: Co (**a**) and Sr (**b**)

Table 4 Summary of adsorption parameters at various temperatures

Model	Parameters	Adsorbates	
		Co	Sr
Freundlich—298 K	K_F (mg/g)/(mg/L)^n	2.467	0.913
	N	10.737	8.032
	R^2	0.738	0.685
Langmuir—298 K	K_L (L/mg)	43.242	1.379
	Q_m (mg/g)	3.304	1.462
	R^2	0.987	0.948
Freundlich—308 K	K_F (mg/g) / (mg/L)^n	3.207	0.726
	N	9.611	3.491
	R^2	0.71	0.852
Langmuir—308 K	K_L (L/mg)	33.447	0.195
	Q_m (mg/g)	4.659	2.54
	R^2	0.968	0.983
Freundlich—318 K	K_F (mg/g)/(mg/L)^n	2.467	0.826
	N	10.737	3.361
	R^2	0.738	0.793
Langmuir—318 K	K_L (L/mg)	12.031	0.136
	Q_m (mg/g)	5.516	3.036
	R^2	0.985	0.969

with 0.979, and 0.948 R^2 respectively, and have maximum adsorption capacities of 3.304 and 1.462 mg/g, respectively. With the adsorption isotherm experiments, one of the research objectives was to confirm the adsorption capacity of BSG for Co and Sr, was achieved successfully. These results also demonstrate the potential use of BSG in the field.

Effect of temperature

Figure 9 shows the results of the temperature experiments, and the specific application parameters are listed in Table 4. When the adsorption temperature increased, the adsorption capacity increased for both Co and Sr. Among the two adsorption models, the Langmuir model was a better fit to the results of both Co and Sr, similar to the previous adsorption isotherm experiments. At 298 K, the adsorption capacities of Co and Sr were 3.268 and 1.462 mg/g, respectively. However, the capacity was increased to 4.659 and 2.54 mg/g, respectively, at 308 K. Moreover, the highest capacity of 5.516 and 3.036 mg/g, respectively, were observed at 318 K. These results

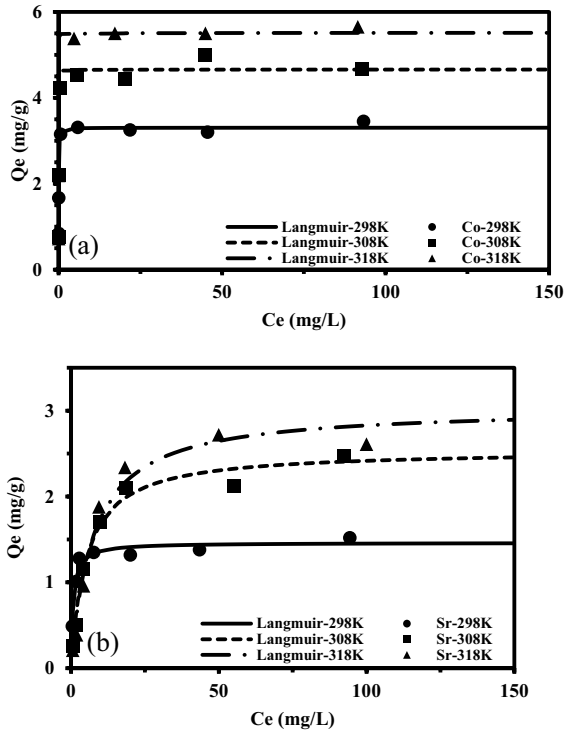

Fig. 9 The changes of the adsorption capacity of BSG-850 at various pH for Co (**a**) and Sr (**b**)

are because higher temperatures can stimulate the chemical reactions and make them faster. In addition, at all temperatures, Co has a higher adsorption capacity than Sr because of its different adsorption affinities, and several studies have shown the same tendencies (Amer et al., 2017; Ivanets et al., 2021; Park et al., 2010; Zhang et al., 2016a, 2016b). These results demonstrate that a higher temperature is more efficient for the adsorption operation of BSG in the field.

To determine the activation energy of BSG, the Arrhenius equation was used (Eq. 6) (Laidler, 1984):

$$k = Ae^{-RT/Ea} \quad (6)$$

where k is the kinetic constant, R is the gas constant, T is the temperature, A is the Arrhenius constant, and E_a is the activation energy. The k value was calculated from the adsorption kinetic data at different temperatures (298, 308, and 318 K), and the activation energies of Co and Sr are listed in Table 5.

Table 5 Summary of activation energies

	Adsorbates					
	Co			Sr		
1/T	0.00335	0.00324	0.00314	0.00335	0.00324	0.00314
ln k	−2.57184	−1.971299	−0.77932	0.058688	2.563949	3.101092
M_w (g/mol)	58.93			87.62		
E_a (kJ/g K)	1.194			1.377		

Table 6 Ionic radius of several competitive ions in this study (Marcus, 1988)

Ion	Radius (pm)
Co^{2+}	210
Sr^{2+}	260
Ni^{2+}	206
Mn^{2+}	219
Cd^{2+}	230
Na^{+}	235

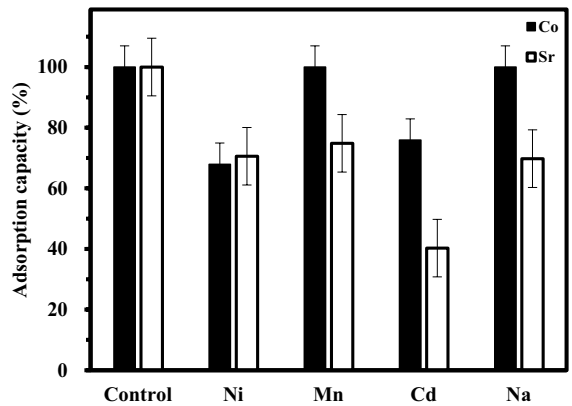

Fig. 10 The changes of the adsorption capacity of BSG-850 at presence of competitive ions

Effect of competitive ions

Similar to the adsorption isotherm experiment, the Langmuir model was a better fit than the Freundlich model, with a higher correlation coefficient. Consequently, the adsorption capacity decreased when other competitive ions were present. In terms of Co, the disturbance effect was Mn (0%) = Na (0%) < Cd (24.1%) < Ni (32.2%) while the disturbance effect of Sr was Mn (25.2%) < Ni (29.4%) < Na (30.2%) < Cd (59.7%). This result might be due to their similar ionic radii and different adsorption affinities. The specific ionic radii are listed in Table 6, and Fig. 10 shows the results for the different adsorption capacities with several competitive ions.

Nickel has similar chemical and physical properties to Co, such as the ionic radius (Ni: 206 pm and Co: 210 pm), and this similarity triggers a disturbance effect in the adsorption process. Cadmium has a relatively higher disturbance effect on both Co and Sr because it has a higher adsorption affinity than other ions (Galedar and Younsei, 2013; Wierzba and Klos, 2019). Sodium does not have any disturbance effect on Co but has a significant effect on Sr. The different effects of Na on Co and Sr and the disturbance effect on Sr are due to the ionic radius (Na: 235 pm, Co: 210 pm, and Sr: 260 pm) (Jang et al., 2018). In addition, the results of Sr show that all of the competitive ions affect the adsorption capacity, and it seems that Sr has a relatively low adsorption affinity. In conclusion, the existence of competitive ions can decrease the adsorption capacity of Co and Sr due to their ionic radii and adsorption affinities. If BSG is applied to the treatment of radioactive waste from NPPs, the dosage should be calculated precisely. In addition, Co, Cd, Ni, and Mn in water are monitoring elements for radioactive waste as well as industrial, agricultural, and drinking water. Therefore, BSG can be applied to the treatment of these types of water to eliminate toxic heavy metals.

Bio-regeneration and potential usage of BSG-origin biochar

After one adsorption operation, the capacities of Co and Sr were decreased to 75.3 and 93.6%, respectively. After continuous 3rd and 4th cycles, the capacities of Co (47.8 and 43.6%, respectively) and Sr (84.2 and 57.2%, respectively) were reduced. The final capacities after the final cycle were 36.2 and 32.7% for Co and Sr, respectively. Both Co and Sr

have a significantly lower capacities than before and have approximately 32–36% of their original capacity after five adsorption operations (Fig. 11).

According to Galedar and Tounsei (2013)**, the adsorption of Co was 0.68 mg/g without any pre-treatment and was much lower than that reported in this study. Since BSG contains radionuclides after the adsorption process, it means that BSG should be treated as radioactive waste. It seems that increasing the adsorption capacity using pretreatment, such as using acid, might be more efficient than the desorption process of BSG.

Table 7 shows the previous study about adsorption of Co and Sr using several materials including activated carbon. Compare to other studies, the adsorption capacity of BSG according to thus research is relatively low, however BSG still has the potential usage as the adsorbent due to the several reasons. First, BSG is the easiest material to gather than other biomasses. As mentioned in upper section, beer is one of the most popular beverage in the world and all counties have their own brewery or beer industry, so there is no big obstacles to get the BSG from them. On the other hand, other biomass like nut shells, or seed of fruit does not saved in one place which means hard to access it. Second, due to the better accessibility, BSG is cheaper than other materials. Third, there is no special pre-treatment to BSG before adsorption process. This means there is a potential of increasing the adsorption capacity with scientific method which can be the direction of following studies.

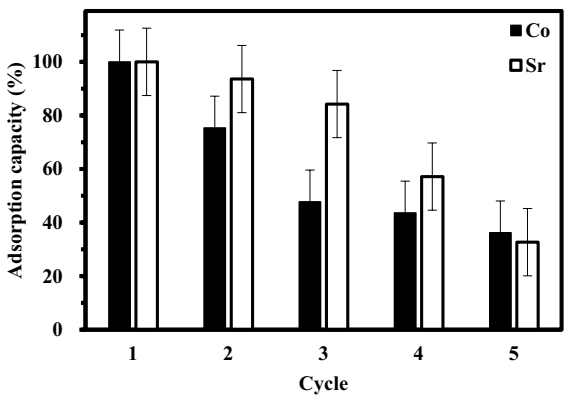

Fig. 11 The changes of the adsorption efficiency of BSG-850 during 5 cycles

Conclusions

With a higher pyrolysis temperature, the surface functional group decreased, which induced a higher pH and lower CEC value. Moreover, after a high level of pyrolysis operation (650–850 °C), the generated biochar had a well-organized C structure like graphite. This result was confirmed by the higher C content and FT-IR analysis. In addition, at higher temperatures, biochar has a larger surface area and more surface pores owing to the degradation of pore-blocking materials and release of volatile matter.

Among the four BSG types (BSG-R, BSG-450, BSG-650, and BSG-850), only BSG-850 had a significant adsorption capacity. The surface area and pore volume might have a greater role and effect than the surface functional groups and BSG-850

Table 7 Comparison of previous and this studies about adsorption capacity

Adsorbent	Adsorption capacity (mg/g)		References
	Co	Sr	
Activated carbon from apricot stone	111.1	–	Abbas et al. (2014)
Activated carbon from lemon peels	22	–	Bhatnagar et al. (2010)
Activated carbon from hazelnut shell	13.88	–	Demirbaş (2003)
Granular activated carbon	1.8	–	Hete et al. (2012)
Chemical modified activated carbon	51.1	–	Kakavandi et al. (2018)
Activated carbon from coconut shell	–	2.02	Caccin et al. (2013)
Granular activated carbon	–	44.4	Chegrouche et al. (2009)
Plant root tissue	–	12.9	Chen (1997)
Activated carbon from banana peels	–	41.5	Mahindrakar and Rathod (2018)
Brewer's spent grain (BSG)	5.516	3.306	This study

had the highest adsorption capacity by adsorption for both Co and Sr at pH 7.

Both Co and Sr adsorption followed PSO in terms of adsorption kinetics and took approximately 24 h to attain the adsorption equilibrium state. In terms of the adsorption isotherms, both follow the Langmuir model with 0.987 and 0.948 R^2 values, respectively at 298 K. The maximum adsorption capacities of Co and Sr at 298 K were calculated as 3.304 and 1.462 mg/g, respectively. With 10 ppm of initial concentration, 298 K, 1.25 g/L of dosage, 200 rpm, and 24 h of shaking, BSG-850 has about 40 and 10% of removal efficiency for Co and Sr, respectively. The pH was maintained as 7 after the adsorption process.

When the adsorption temperature increased, the adsorption capacities of Co and Sr also increased and still followed the Langmuir model. At 298 K, BSG had 3.304 and 1.462 mg/g capacities for Co and Sr, respectively, but increased to 4.659 and 2.54 mg/g for Co and Sr, respectively. The highest adsorption capacities (5.516. mg/g for Co and 3.036 mg/g for Sr) was observed at the highest adsorption temperature of 318 K.

The adsorption of Co and Sr was disturbed by other competitive ions such as Ni, Mn, Cd, and Na. In terms of Co, the disturbance effect was Mn (0%) = Na (0%) < Cd (24.1%) < Ni (32.2%), whereas the Sr disturbance effect was Mn (25.2%) < Ni (29.4%) < Na (30.2%) < Cd (59.7%).

The reusability of BSG was observed by comparing its adsorption capacity after five adsorption and desorption operations. The adsorption capacities for Co and Sr decreased to 75.3 and 93.6% after the 1st cycle. After the 2nd and 3rd cycles, the adsorption capacities of Co (47.8 and 43.6%, respectively) and Sr (84.2 and 57.2%, respectively) decreased. After the final cycle, the capacities were 36.22% for Co and 32.7% for Sr, respectively.

Acknowledgements This work was supported by the National Research Foundation of Korea (NRF) grant funded by the Korea government (MSIT) (No. 2021R1A2C1094272).

Author contributions H-WL: Conceptualization, Investigation, Methodology, Formal analysis, Writing—original draft. H-GJ: Conceptualization, Methodology, Supervision, Laboratory support. K-WK: Supervision, Validation, Writing—review and editing.

Funding National Research Foundation of Korea (NRF) grant funded by the Korea government (MSIT) (No. 2021R1A2C1094272).

Declarations

Conflict of interest The authors have not disclosed any competing interests.

References

Abbas, M., Kaddour, S., & Trari, M. (2014). Kinetic and equilibrium studies of cobalt adsorption on apricot stone activated carbon. *Journal of Industrial and Engineering Chemistry, 20*(3), 745–751. https://doi.org/10.1016/j.jiec.2013.06.030

Ahmad, M., Rajapaksha, A. U., Lim, J. E., Zhang, M., Bolan, N., Mohan, D., & Ok, Y. S. (2014). Biochar as a sorbent for contaminant management in soil and water: A review. *Chemosphere, 99*, 19–33. https://doi.org/10.1016/j.chemosphere.2013.10.071

Amer, H., Moustafa, W. M., Farghali, A. A., El Rouby, W. M., & Khalil, W. F. (2017). Efficient removal of Cobalt (II) and Strontium (II) Metals from water using ethylene diamine tetra-acetic acid functionalized graphene oxide. *Zeitschrift Für Anorganische Und Allgemeine Chemie, 643*(22), 1776–1784. https://doi.org/10.1002/zaac.201700318

Bachmann, S. A. L., Calvete, T., & Féris, L. A. (2022). Potential applications of brewery spent grain: Critical an overview. *Journal of Environmental Chemical Engineering, 10(1),* 106951. https://doi.org/10.1016/j.jece.2021.106951

Balogun, A. O., Sotoudehniakarani, F., & McDonald, A. G. (2017). Thermo-kinetic, spectroscopic study of brewer's spent grains and characterisation of their pyrolysis products. *Journal of Analytical and Applied Pyrolysis, 127*, 8–16. https://doi.org/10.1016/j.jaap.2017.09.009

Bhatnagar, A., Minocha, A. K., & Sillanpää, M. (2010). Adsorptive removal of cobalt from aqueous solution by utilizing lemon peel as biosorbent. *Biochemical Engineering Journal, 48*(2), 181–186. https://doi.org/10.1016/j.bej.2009.10.005

Caccin, M., Giacobbo, F., Da Ros, M., Besozzi, L., & Mariani, M. (2013). Adsorption of uranium, cesium and strontium onto coconut shell activated carbon. *Journal of Radioanalytical and Nuclear Chemistry, 297*, 9–18. https://doi.org/10.1007/s10967-012-2305-x

Chegrouche, S., Mellah, A., & Barkat, M. (2009). Removal of strontium from aqueous solutions by adsorption onto activated carbon: Kinetic and thermodynamic studies. *Desalination, 235*(1–3), 306–318. https://doi.org/10.1016/j.desal.2008.01.018

Chen, J. P. (1997). Batch and continuous adsorption of strontium by plant root tissues. *Bioresource Technology, 60*(3), 185–189. https://doi.org/10.1016/S0960-8524(97)00021-7

Demirbaş, E. (2003). Adsorption of cobalt (II) ions from aqueous solution onto activated carbon prepared from hazelnut shells. *Adsorption Science and Technology, 21*(10), 951–963. https://doi.org/10.1260/026361703607443380

Galedar, M., & Younesi, H. (2013). Biosorption of ternary cadmium, nickel and cobalt ions from aqueous solution onto Saccharomyces cerevisiae cells: Batch and column studies. *American Journal of Biochemistry and Biotechnology, 9*(1), 47. https://doi.org/10.3844/ajbbsp.2013.47.60

Hassan, S. S., Ravindran, R., Jaiswal, S., Tiwari, B. K., Williams, G. A., & Jaiswal, A. K. (2020). An evaluation of sonication pretreatment for enhancing saccharification of brewers' spent grain. *Waste Management, 105*, 240–247. https://doi.org/10.1016/j.wasman.2020.02.012

Hete, Y. V., Gholase, S. B., & Khope, R. U. (2012). Adsorption study of cobalt on treated granular activated carbon. *E-Journal of Chemistry, 9*(1), 335–339. https://doi.org/10.1155/2012/472517

Ivanets, A., Radkevich, A., Shashkova, I., Kitikova, N., Zarubo, A., & Venhlinskaya, E. (2021). Study of dynamic adsorption and desorption kinetics of cesium, strontium, cobalt radionuclides on granular phosphate adsorbent. *Journal of Radioanalytical and Nuclear Chemistry, 327*(3), 1291–1298. https://doi.org/10.1007/s10967-020-07584-w

Jang, J., Miran, W., Divine, S. D., Nawaz, M., Shahzad, A., Woo, S. H., & Lee, D. S. (2018). Rice straw-based biochar beads for the removal of radioactive strontium from aqueous solution. *Science of the Total Environment, 615*, 698–707. https://doi.org/10.1016/j.scitotenv.2017.10.02

Kakavandi, B., Raofi, A., Peyghambarzadeh, S. M., Ramavandi, B., Niri, M. H., & Ahmadi, M. (2018). Efficient adsorption of cobalt on chemical modified activated carbon: Characterization, optimization and modeling studies. *Desalination and Water Treatment, 111*, 310–321. https://doi.org/10.5004/dwt.2018.22238

Kwak, J. H., Islam, M. S., Wang, S., Messele, S. A., Naeth, M. A., El-Din, M. G., & Chang, S. X. (2019). Biochar properties and lead (II) adsorption capacity depend on feedstock type, pyrolysis temperature, and steam activation. *Chemosphere, 231*, 393–404. https://doi.org/10.1016/j.chemosphere.2019.05.128

Laidler, K. J. (1984). The development of the Arrhenius equation. *Journal of Chemical Education, 61*(6), 494. https://doi.org/10.1021/ed061p494

Langmuir, I. (1918). The adsorption of gases on plane surfaces of glass, mica and platinum. *Journal of the American Chemical Society, 40*(9), 1361–1403. https://doi.org/10.1021/ja02242a004

Li, S., Harris, S., Anandhi, A., & Chen, G. (2019). Predicting biochar properties and functions based on feedstock and pyrolysis temperature: A review and data syntheses. *Journal of Cleaner Production, 215*, 890–902. https://doi.org/10.1016/j.jclepro.2019.01.106

Liu, Y., He, Z., & Uchimiya, M. (2015). Comparison of biochar formation from various agricultural by-products using FTIR spectroscopy. *Modern Applied Science, 9*(4), 246. https://doi.org/10.5539/mas.v9n4p246

Mahindrakar, K. V., & Rathod, V. K. (2018). Utilization of banana peels for removal of strontium (II) from water. *Environmental Technology and Innovation, 11*, 371–383. https://doi.org/10.1016/j.eti.2018.06.015

Masson-Delmotte, V., Zhai, P., Pörtner, H. O., Roberts, D., Skea, J., Shukla, P. R., & Waterfield, T. (2018). Global warming of 1.5 C. *An IPCC Special Report on the impacts of global warming of, 1(5),* 43–50. https://doi.org/10.1017/9781009157940.011

Marcus, Y. (1988). Ionic radii in aqueous solutions. *Chemical Reviews, 88*(8), 1475–1498.

Mussatto, S. I., Dragone, G., & Roberto, I. C. (2006). Brewers' spent grain: Generation, characteristics and potential applications. *Journal of Cereal Science, 43*(1), 1–14. https://doi.org/10.1016/j.jcs.2005.06.001

Osman, A. I., O'Connor, E., McSpadden, G., Abu-Dahrieh, J. K., Farrell, C., Al-Muhtaseb, A., & Rooney, D. W. (2019). Upcycling brewer's spent grain waste into activated carbon and carbon nanotubes via two-stage activation for energy and other applications. *Journal of Chemical Technology & Biotechnology., 95*, 183. https://doi.org/10.1002/jctb.6220

Park, Y., Lee, Y. C., Shin, W. S., & Choi, S. J. (2010). Removal of cobalt, strontium and cesium from radioactive laundry wastewater by ammonium molybdophosphate–polyacrylonitrile (AMP–PAN). *Chemical Engineering Journal, 162*(2), 685–695. https://doi.org/10.1016/j.cej.2010.06.026

Qiu, H., Vijver, M. G., He, E., & Peijnenburg, W. J. (2013). Predicting copper toxicity to different earthworm species using a multicomponent Freundlich model. *Environmental Science and Technology, 47*(9), 4796–4803. https://doi.org/10.1021/es305240n

Tomczyk, A., Sokołowska, Z., & Boguta, P. (2020). Biochar physicochemical properties: Pyrolysis temperature and feedstock kind effects. *Reviews in Environmental Science and Bio/technology, 19*, 191–215. https://doi.org/10.1007/s11157-020-09523-3

Vanderheyden, S. R. H., Vanreppelen, K., Yperman, J., Carleer, R., & Schreurs, S. (2018). Chromium (VI) removal using in-situ nitrogenized activated carbon prepared from Brewers' spent grain. *Adsorption, 24*, 147–156. https://doi.org/10.1007/s10450-017-9929-7

Wierzba, S., & Kłos, A. (2019). Heavy metal sorption in biosorbents–Using spent grain from the brewing industry. *Journal of Cleaner Production, 225*, 112–120. https://doi.org/10.1016/j.jclepro.2019.03.286

Zhang, L., Wei, J., Zhao, X., Li, F., Jiang, F., Zhang, M., & Cheng, X. (2016a). Competitive adsorption of strontium and cobalt onto tin antimonate. *Chemical Engineering Journal, 285*, 679–689. https://doi.org/10.1016/j.cej.2015.10.013

Zhang, L., Wei, J., Zhao, X., Li, F., Jiang, F., Zhang, M., & Cheng, X. (2016b). Removal of strontium (II) and cobalt (II) from acidic solution by manganese antimonate. *Chemical Engineering Journal, 302*, 733–743. https://doi.org/10.1016/j.cej.2016.05.040